Synthesis, photophysical evaluation, and computational study of 2-methoxy- and 2-morpholino pyridine compounds as highly emissive fluorophores in solution and the solid state

Masayori Hagimori,[a,*] Yasuhisa Nishimura,[b] Naoko Mizuyama,[c] and Yasuhiro Shigemitsu,[b,d,*]

[a]Graduate School of Biomedical Sciences, Nagasaki University, 1-7-1 Sakamoto, Nagasaki 852-8501, Japan

[b]Graduate School of Engineering, Nagasaki University, 1-14, Bunkyo-machi, Nagasaki 852-8131, Japan

[c]Clinical Research Center, Nagasaki University Hospital, 1-7-1 Sakamoto, Nagasaki 852-8501, Japan

[d]Industrial Technology Center of Nagasaki, 2-1303-8, Ikeda, Omura, Nagasaki 856-0026, Japan

Author E-mail address: hagimori@nagasaki-u.ac.jp (M Hagimori); shige@tc.nagasaki.go.jp (Y Shigemitsu)

*Corresponding author.

Abstract

Two 2-pyridone tautomeric analogs, methoxypyridine **4** and *N*-methylpyridone **5**, were synthesized, and their spectroscopic properties were investigated both experimentally and computationally. A detailed photophysical study reveals that **4** shows high fluorescence quantum yields not only in chloroform but also in ethanol, and the strong fluorescence in solution might be attributed to the enol form (pyridine) of the 2-pyridone. Furthermore, we designed and synthesized novel 2-substitued pyridines to achieve more intense emissions in both solution and the solid state. Substituent modification with phenylsulfonyl, morpholino, and 4-diethylamino groups greatly affected the fluorescence properties, and methoxypyridine **7** and morpholinopyridine compound **8** showed fluorescence in various solvents (Φ = 0.59–0.95) and the solid state (Φ = 0.12–0.15). A hypsochromic shift in the emission maximum wavelength and strong fluorescence in the solid state (Φ = 0.39) were observed for dimorpholinopyridine **9**. Morpholinopyridine **11** showed intense fluorescence in all nonpolar and polar solvents. Systematic time-dependent density functional theory calculations were performed for the compounds whose electronic and fluorescent maxima were computationally reproduced with good agreement to those from experiment. In detail, the drastic difference in the emission intensity between **4** and **5** in solution was successfully explained using CASSCF calculations, which revealed conical intersections between the ground and the excited states.

Keywords: 2-Pyridone, keto–enol tautomerism, pyridine, fluorescence in solution, fluorescence in the solid state, TDDFT, CASSCF, conical intersection

1. Introduction

Fluorophores are one of the most useful materials in various chemical, biological, and material sciences because of their sensitivity, simplicity, color tunability, and low cost [1–3]. Each fluorophore, which could be an organic molecule, fluorescent protein, or quantum dot, for example, has a specific wavelength of absorbance and emission of light from the visible to near infrared region [1,4–6]. In organic molecules, particularly heterocyclic compounds, these fluorescence characteristics can be easily tuned by chemical modification [7,8]. Therefore, there has been significant effort to develop fluorophores based on organic molecules for applications as clinical diagnostic probes and organic light-emitting materials [9–11].

2-Pyridone is a nitrogen-containing heterocyclic compound and is used as a scaffold for antibacterial, anticancer, antiviral, and antimalarial agents [12–15]. In addition, 2-pyridone-based fluorophores exhibiting strong fluorescence have been reported [16–18]. Previously, we also reported several fluorescent 2-pyridone compounds, 6-(4-dialkylamino)phenyl-2-pyridones, that exhibit aggregation-induced emission enhancement (AIEE)-based fluorescence in the solid state [19,20]. These 2-pyridone compounds also exhibited fluorescence in solution, and the fluorescence quantum yields (Φ) in chloroform were very high (Φ = 0.90–0.92) [20]. However, the fluorescence intensity of the 2-pyridone compounds decreased in polar solvents such as ethanol (Φ = 0.11–0.22) [20]. It has been reported that the 2-pyridone ring has two tautomeric forms (keto and enol); the favored form depends on the solvent polarity. The 2-hyroxypyridine enol form is favored in nonpolar solvents, whereas the 2-pyridone keto form is favored in polar solvents [21–24]. Therefore, we assumed that the tautomerism of the 2-pyridone ring affects the fluorescence intensity in nonpolar and polar solvents.

Thus, to elucidate this hypothesis, we synthesized 2-pyridone tautomeric analogs, methoxypyridine compound **4** and *N*-methylpyridone compound **5**, and characterized their

fluorescence properties using photophysical studies, as well as quantum chemical calculations. We have found that the enol form greatly contributes to the fluorescence intensity in both nonpolar and polar solvents. In heterocyclic compounds, the arrangement of the electron-donating or electron–withdrawing groups affects the intramolecular charge transfer (ICT) and enhances the fluorescence intensity [18,25–27]. In addition, we reported that the steric hindrance of the alkyl group reduces the molecular aggregation of 2-pyridone and induced AIEE-based fluorescence [18,19]. Most AIEE materials previously reported exhibited strong fluorescence in the solid state, but their fluorescence in solution was very weak [28]. Therefore, the development of fluorophores exhibiting fluorescence in both solution and the solid state has attracted attention. In this paper, we report the synthesis and characterization of novel 2-substituted pyridine compounds (**7**–**9** and **11**) that exhibit strong fluorescence in various solvents and the solid state.

2. Materials and methods

All chemicals were reagent grade and used without further purification unless otherwise specified. The identification of new compounds and the measurement of the fluorescence properties were performed with the following equipment. Melting points were measured using a Laboratory Devices Mel-Temp II apparatus and a Mitamura Riken Kogyo Mel-Temp apparatus. The NMR spectra of the compounds were obtained using Gemini 300NMR (300 MHz) and JEOL-GX-400 (400 MHz) spectrometers. Mass spectra (MS) and high-resolution (HR) MS were obtained using a JEOL DX-303 mass spectrometer. Elemental microanalyses were recorded using a Perkin-Elmer CHN analyzer.

2.1 Synthesis of

*6-(4-dimethylamino)phenyl-4-methylsulfanyl-2-methoxypyridine-3-carbonitrile (**4**) and*

*6-(4-dimethylamino)phenyl-1-methyl-4-methylsulfanyl-3-cyano-2H-pyridone (**5**)*

As described previously [20], 6-(4-(dimethylamino)phenyl)-4-(methylsulfanyl)-2-oxo-1,2-dihydropyridine-3-carbonitrile (**3**; 86 mg, 0.29 mmol, 29%) was prepared by the reaction of 4'-dimethylaminoacetophenone (**1a**; 1.63 g, 10.0 mmol) and 3,3-bis(methylsulfanyl)malononitrile (**2a**; 2.86 g, 10.0 mmol) using powdered NaOH (1.60 g, 40 mmol) as a base in dimethyl sulfoxide (DMSO, 20 mL). To a suspension of **3** (285 mg, 1.0 mmol) in DMSO (5.0 mL) and 2 N sodium hydroxide (3.0 mL), dimethyl sulfate (189 mg, 1.5 mmol) was added over 20 min, and the resulting suspension was stirred for 1.5 h. After pouring 50 mL water into the reaction mixture, a precipitate formed, which was collected by filtration and washed several times with water. Purification by silica gel column chromatography (10 g of silica gel) eluted with toluene gave **4** (86 mg, 0.29 mmol, 29%) and that with toluene and methanol (ratio 4:1) gave **5** (107 mg, 0.36 mmol, 36%). An analytical sample was recrystallized from methanol to give pale yellow needles of **4** (mp 171–172 °C). IR (KBr, cm^{-1}): 2921, 2211, 1609, 1566, 1539, 1364, 1187, 1166, 1034, 812. ^{1}H-NMR ($CDCl_3$, 400 MHz): 2.62 (3H, s, SMe), 3.06 (6H, s, NMe_2), 4.11 (3H, s, OMe), 6.75 (2H, d, J = 9.1 Hz, 3', 5'-H), 7.06 (1H, s, 5-H), 7.96 (2H, d, J = 9.1 Hz, 2', 6'-H). ^{13}C-NMR ($CDCl_3$, 100 MHz): 14.4, 41.3, 54.2, 106.4, 114.5, 128.7, 157.1, 164.4. MS m/z: 300 (M^+ + 1, 70), 299 (M^+, 100), 298 (83), 282 (11), 240 (22), 236 (11). Anal. Calcd for $C_{16}H_{17}N_3SO$ = 299.1092: C, 64.19%; H, 5.72%; N, 14.04%. Found: C, 64.36%; H, 5.74%; N, 14.10%. An analytical sample was recrystallized from methanol to give yellow needles of **5** (mp 218–220 °C). IR (KBr, cm^{-1}): 3250, 3000, 2910, 2820, 2210 (CN), 1640 (C=O), 1600, 1510, 1490, 1440, 1420, 1360, 1310, 1290, 1240, 1215, 1180, 1060, 1040. ^{1}H-NMR ($CDCl_3$, 400 MHz): 2.52 (3H, s, Me), 3.07 (6H, s, NMe_2), 3.44 (3H, s, NMe), 6.05 (1H, s, 5-H), 6.80 (2H, d,

119 J = 9.1 Hz, 3',5'-H), 7.27 (2H, d, J = 9.1 Hz, 2', 6'-H). ^{13}C-NMR ($CDCl_3$, 100 MHz): 14.4,
120 34.9, 40.3, 95.68, 103.5, 111.9, 115.0, 129.3, 151.2, 154.3, 160.7, 161.1. MS m/z: 300 (M^+ + 1,
121 47), 299 (M^+, 100), 298 (13), 127 (11), 112 (12), 99 (15). Anal. Calcd for $C_{16}H_{17}N_3SO$ =
122 299.1092: C, 64.19%; H, 5.72%; N, 14.04%. Found: C, 64.01%; H, 5.68%; N,13.86%.
123
124 *2.2 Synthesis of*
125 *6-(4-dimethylamino)phenyl-4-methylsulfanyl-3-phenylsulfonyl-2-methoxypyridine (**7**)*
126 As described previously [20],
127 6-(4-(dimethylamino)phenyl)-4-(methylsulfanyl)-3-(phenylsulfonyl)pyridin-2(1H)-one (**6**)
128 (0.96 g, 2.40 mol) was prepared by the reaction of **1a** (1.63 g, 10.0 mmol) and
129 3,3-bis(methylsulfanyl)-2-phenylsulfonyl-acrylonitrile (**2b**; 1.43 g, 5.0 mmol) using powdered
130 NaOH (1.12 g, 28 mmol) and morpholine (1.5 g, 17.2 mmol) in DMSO (20 mL). To a
131 suspension of **6** (150 mg, 3.75 mmol) in DMSO (10 mL) and a solution of 1 N sodium
132 hydroxide (6.0 mL), dimethyl sulfate (250 mg, 1.5 mmol) was added over 30 min, and the
133 resulting suspension was stirred for 1.5 h. After the addition of 50 mL water to the reaction
134 mixture, the formed precipitate was collected by filtration and washed several times with water.
135 Purification by silica gel column chromatography (10 g of silica gel) eluted with toluene gave
136 pale yellow needles of **7** (65 mg, 0.157 mmol, 42%, mp 194–195 °C). IR (KBr, cm^{-1}): 2920,
137 2367, 2337, 1615, 1527, 669. ^{1}H-NMR ($CDCl_3$, 400 MHz): 2.55 (3H, s, Me), 3.07 (6H, s,
138 NMe_2), 3.93 (3H, s, OMe), 6.73 (2H, d, J = 9.3 Hz, 3",5"-H), 7.11 (1H, s, 5-H), 7.48 (2H, m,
139 3',5'-H), 7.56 (1H, m, 4'-H), 7.91 (2H, d, J = 9.3 Hz, 2",6"-H), 8.06 (2H, m, 2',6'-H).
140 ^{13}C-NMR ($CDCl_3$, 100 MHz): 16.0, 16.1, 40.1, 40.1, 53.8, 107.0, 107.1, 111.7, 124.5, 127.6,
141 128.2, 128.4, 142.7, 151.8, 155.8, 157.4, 160.9. MS (FAB) m/z: 415 ($M + H^+$).
142

*2.3 Synthesis of 6-(4-(dimethylamino)phenyl)-4-(methylsulfanyl)-2-morpholinonicotinonitrile (**8**) and 6-(dimethylamino)phenyl-2,4- dimorpholinopyridine-3-carbonitrile (**9**)*

A solution of **1a** (1.63 g, 10.0 mmol), **2a** (2.86 g, 10.0 mmol), and NaOH (1.60 g, 40 mmol) in DMSO (20 mL) was stirred at 10–15 °C for 5 h. After the addition of 300 mL of ice water to the reaction mixture, the mixture was acidified with 10% hydrochloric acid. The resulting caramel-colored intermediate was collected by decantation and washed with ice cold water several times. A solution of the intermediate in water and morpholine (3.0 g, 34.4 mmol) was heated for 20 min at about 200 °C. After filtration, the filtrate was concentrated in vacuo. Purification by silica gel column chromatography (20 g of silica gel) eluted with toluene:methanol (4:1) gave **3** (960 mg, 2.40 mmol, 24%), **8** (92 mg, 0.26 mmol, 2.6%), and **9** (82 mg, 0.21 mmol, 2.1%). An analytical sample was recrystallized from methanol to give colorless needles of **8** (mp 167–168 °C). IR (KBr, cm^{-1}): 2854, 2367, 2336, 1570, 1532, 1112. ^{1}H-NMR ($CDCl_3$, 400 MHz): 3.04 (6H, s, NMe_2), 3.42 (2H, m, N–CH_2–), 3.70 (2H, m, N–CH_2–), 3.87 (4H, m, –CH_2–O–CH_2–), 6.73 (2H, d, J = 8.8 Hz, 3', 5'-H), 7.91 (2H, d, J = 8.8 Hz, 2', 6'-H). ^{13}C-NMR ($CDCl_3$, 100 MHz): 14.5, 40.4, 48.8, 66.8, 89.3, 104.9, 112.2, 116.8, 128.5, 157.3, 157.4, 161.6. MS *m*/*z*: 355 (M^+ + 1, 28), 354 (M^+, 100), 339 (14), 324 (16), 323 (20), 297 (60), 296 (87), 269 (14), 222 (11). Anal. Calcd for $C_{19}H_{22}N_4SO$ = 354.1514: C, 64.38%; H, 6.26%; N, 15.81%. Found: C, 64.32%; H, 6.22%; N, 15.85%. In addition, an analytical sample was recrystallized from methanol to give colorless needles of **9** (mp 197–198 °C). IR (KBr, cm^{-1}): 2966, 2851, 2193 (CN), 1608, 1570, 1536, 1112, 819. ^{1}H-NMR ($CDCl_3$, 400 MHz): 3.04 (6H, s, NMe_2), 3.44 (4H, m, 2 × N–CH_2–), 3.70 (4H, m, 2 × N–CH_2–), 3.88 (8H, m, 2 × O–CH_2–). ^{13}C-NMR ($CDCl_3$, 100 MHz): 40.4, 49.2, 50.6, 66.6, 66.8, 82,3, 98.2, 112.0, 118.8, 128.3, 158.9, 163.7, 163.9. MS *m*/*z*: 394 (M^+ + 1, 24), 393 (M^+, 94), 336 (41), 335 (100), 315 (16), 299 (29). Anal. Calcd for $C_{22}H_{27}N_5O_2$ = 393.2165: C, 67.15%; H, 6.92%; N, 17.80%. Found: C, 67.01%; H, 7.05%; N, 17.77%.

2.4 Synthesis of

*6-(4-diethylamino)phenyl-4-methylsulfanyl-2-morpholinopyridine-3-carbonitrile (**11**)*

Compound **11** (54 mg 0.141 mmol, 2.8% yield) was prepared from 4-(diethylamino)phenylacetophenone (**1b**, 0.86 g, 5.0 mmol) and **2a** (0.85 g, 5.0 mmol) in a manner similar to that described for the synthesis of **8**. An analytical sample was recrystallized from dimethylformamide (DMF) and methanol to give pale yellow needles (mp 137–138 °C). IR (KBr, cm^{-1}): 2898, 2845, 2200 (CN), 1608, 1537, 1524, 1419, 1366, 814. ^{1}H-NMR ($CDCl_3$, 400 MHz): 1.21 (6H, t, J = 7.0 Hz, 2 × CH_2-$\underline{CH_3}$), 2.60 (3H, s, SMe), 3.43 (4H, d, J = 7.0 Hz, 2 × N-CH_2-), 3.73 (4H, t, J = 5.1 Hz, 2 × -CH_2-N), 3.68 (4H, t, J = 5.1 Hz, 2 × O-CH_2-), 6.71 (2H, d, J = 9.2 Hz, 3', 5'-H), 6.93 (1H, s, 5-H), 7.91 (2H, d, J = 9.1 Hz, 2', 6'-H). ^{13}C-NMR (DMSO-d6, 100MHz): 12.4, 13.6, 43.7, 48.5, 65.94, 87.5, 104.6, 110.9, 116.6, 123.1, 129.0, 149.1, 156.7, 157.2, 161.1. Anal. Calcd for $C_{21}H_{22}N_2S_2O_3$ = 382.1827: C, 65.94%; H, 6.85%; N, 14.65%. Found: C, 65.78%; H, 6.76%; N, 14.63%.

2.5. Fluorescence measurements

The solid-state fluorescence of powdered samples was measured in a Shimadzu RF-5300pc fluorescence spectrometer. After the excitation spectrum had been measured by scanning at the fluorescent wavelength, the fluorescence spectrum was obtained using the excitation wavelength. The fluorescence spectra in solution were obtained in a manner similar to that in the solid state. To measure the fluorescence in solution, the concentrations of samples were adjusted using a molar absorption coefficient of 0.05. The fluorescence spectra in solution were obtained in the same way as the solid-state measurements. Fluorescence quantum yields were determined using an Absolute PL Quantum Yield Measurement System (C9920-01) from Hamamatsu Photonics.

193

194 *2.6. X-ray crystallography*

195 X-ray diffractometry (XRD) data were obtained with a Rigaku Saturn724 diffractometer using
196 multilayer mirror monochromated Mo-Kα radiation at -179 ± 1 °C, and all calculations were
197 conducted using CrystalClear (Rigaku). The structure of **8** (CCDC-1896939) can be obtained
198 from the Cambridge Crystallographic Data Centre via request
199 (www.ccdc.cam.au.uk/data_request/cif).
200 Crystal data for **8**: A crystal was obtained by recrystallization from MeOH/acetonitrile (1:1),
201 which yielded colorless blocks of formula $C_{19}H_{22}N_4OS$ having approximate dimensions of
202 0.270 × 0.080 × 0.020 mm. The crystal was mounted on a glass fiber for data collection.
203 Crystal data formula weight: 354.47; crystal color: colorless; habit: block; crystal system:
204 triclinic; lattice type: primitive; lattice parameters: a = 11.072(3) Å, b = 11.374(3) Å, c =
205 15.493(4) Å, β = 90.259(3)°, V = 1819.7(7) Å^3; space group: P-1 (#2); Z-value: 4; calculated
206 density (D_{calcd}): 1.294 g cm^{-3}; F(000) = 752.00; and absorption coefficient (μ(Mo-Kα)) = 1.923
207 cm^{-1}.
208

209 **3. Computational details**

210 The ground state geometries of all molecules in vacuo were fully optimized at the density
211 functional theory (DFT) B3LYP/6-311++G(d,p) level of theory. The lowest excited states (S_1)
212 were geometrically optimized in vacuo by means of time-dependent DFT (TDDFT)
213 calculations at the B3LYP/6-31+G(d,p) level of theory using the default convergence criterion
214 for force and displacement implemented in Gaussian 09 [29]. For the optimized geometries, the
215 S_0–S_1 (absorption) and the S_1–S_0 transition energies (fluorescence) were evaluated at the
216 TDDFT/6-311++G(d,p) and 6-31+(d,p) levels using the B3LYP [30], CAM-B3LYP [31],
217 PBEPBE [32], M06 [33], and M06-2X [33] exchange–correlation (XC) functionals. Solvent

effects were taken into account using the polarizable continuum model (PCM).

In the detailed study of **4** and **5**, the relaxation paths in S_1 were explored from the Franck–Condon (FC) state to the S_1-minimum and to the minimum energy conical intersections (MECIs) [34], respectively. The MECIs were located using MOLPRO [35] at the CASSCF(8,7)/def2-SV(P) level of theory. The single point calculations were carried out at the TDDFT(B3LYP)/def-TZVP level of theory using the TURBOMOLE suite of program [36] to refine the energies of the S_1-FC, the S_1-minima, and the S_0/S_1-MECIs states.

4. Results and discussion

*4.1 Synthesis and fluorescence of 2-pyridone tautomeric analogs (**4** and **5**)*

The synthesis of 2-methoxypyridine compound **4** and *N*-methylpyridone compound **5** is shown in Scheme 1. The reaction of 4'-dimethylaminoacetophenone (**1a**) with cyano-keten *S,S*-acetal (**2a**) in the presence of sodium hydroxide as a base in DMSO at room temperature followed by the addition of 10% hydrochloric acid yielded 2-pyridone compound **3** in 29%. The methylation of **3** was achieved using dimethyl sulfate in the presence of sodium hydroxide, and the resultant mixture of **4** and **5** was easily separated by silica gel column chromatography. Methoxypyridine compound **4** was firstly eluted using toluene in 29% yield, and *N*-methylpyridone compound **5** was subsequently eluted using a mixture of toluene and methanol (ratio 4:1) in 36% yield. Next, we analyzed the fluorescence properties of these compounds in two solutions (chloroform and ethanol) and the solid state. The absorption maxima (λ_{max}), emission maxima (Em_{max}), and Φ values of compounds **3**–**5** are listed in Table 1. The Em_{max} values of **4** and **5** were observed at 461 nm in chloroform and at 491 nm in ethanol, which is a hypsochromic shift of the same extent as that induced by the *N*- or *O*-methylation of **3**. Methoxypyridine compound **4** exhibited strong fluorescence both in chloroform ($\Phi > 0.99$) and ethanol ($\Phi = 0.61$), whereas the Φ values of *N*-methylpyridone

compound **5** were very low in both chloroform (Φ = 0.12) and ethanol (Φ = 0.05). Because the fluorescence of 2-pyridone **3** was intense in chloroform (Φ = 0.90) but weak in ethanol (Φ = 0.11), we speculated that the fluorescence of 2-pyridones in chloroform is due to the pyridine form (the enol of 2-pyridone), whereas that in ethanol is due to the pyridone form (the keto of 2-pyridone). In the solid state, the Em_{max} values of **4** and **5** also occurred at shorter wavelengths than that of **3**; however, *N*-methylpyridone compound **5** exhibited stronger fluorescence (Φ = 0.18) than methoxypyridine compound **4** (Φ = 0.03). In a previous study, we revealed that 2-pyridones, including compound **3** (Φ = 0.17), show moderate fluorescence in the solid state, and we also reported that the keto–enol equilibrium of these 2-pyridones is remarkably shifted to the 2-pyridone tautomer on the basis of X-ray crystal structure analysis [20]. Therefore, the fluorescence intensity of **5** in the solid state is consistent with our previous results.

Scheme 1.

Table 1.

4.2 Synthesis and fluorescence of 2-substituted pyridines

The molecular packing arrangement and orientation caused by substituents often influence the fluorescence intensity in the solid state [20,28]. We previously reported that the introduction of sulfonyl group disrupts the molecular planarity of 2-pyridones, thus decreasing the π—π stacking interactions [20,37]. Therefore, compounds showing strong fluorescence in both solution and the solid state could be developed by introducing a substituent into the pyridine that exhibits strong fluorescence in solution. Thus, we prepared a series of 2-substitued pyridine compounds: **7**–**9** and **11** (Scheme 2). After sulfonyl pyridone

compound **6** had been prepared from the reaction of **1a** with **2b**, the methylation of 6 using dimethyl sulfate was conducted, similar to the syntheses of **4** and **5**. In this reaction, however, methoxypyridine compound **7** was only obtained in 42% yield. Morpholinopyridine compounds **8** and **9** were prepared from **1a** and **2a** using morphine. After filtration the major products, 3,2-morpholinopyridine compound **8** and 2,4-dimorpholinopyridine compound **9**, were obtained from the filtrate in 2.6% and 2.1% yields, respectively. Fig. 1 shows the X-ray crystal structure of compound **8**. We previously reported that the replacement of the dimethylamino group with a diethylamino group at the 6-positon of the 2-pyridone ring reduces the molecular aggregation, and diethylamino 2-pyridone compound **10** showed stronger fluorescence than dimethylamino 2-pyridone compound **3** in solution [20,38]. 6-(4-Diethylamino)phenyl-2-morpholinopyridine compound **11** was obtained in a similar manner from the reaction of **1b** and **2a**.

The fluorescence properties of **7**–**9** and **11** in solution (chloroform and ethanol) and the solid state are summarized in Table 2. The Φ values of phenylsulfonyl-methoxypyridine compound **7** were 0.95 in chloroform and 0.62 in ethanol, which are comparable to that of methoxypyridine compound **4**. Meanwhile, the solid state fluorescence of **7** was increased to 0.15, suggesting that molecular planarity disruption is induced by the introduction of the phenylsulfonyl group, as in the 2-pyridones [20]. Compounds **8** and **9** contain a morpholino group instead of a methoxy group and also exhibited strong fluorescence in the solid state, especially dimorpholinopyridine compound **9**, which showed intense fluorescence (Φ = 0.39). In contrast, the Φ values in solution decreased with increasing number of morpholino groups. The Em_{max} of **9** exhibits hypsochromic shifts about 50–65 nm in solution. 4-Diethylamino morpholinopyridine compound **11** exhibited stronger fluorescence than 4-dimethylamino morpholinopyridine compound **8** in solution and the solid state. The emission maximum

wavelengths of **11** in chloroform and ethanol were hypsochromically shifted by about 25 nm, and, interestingly, the solid state emission wavelength was bathochromically shifted by about 55 nm.

4.3 Solvatochromic effects on absorption and emission

The fluorescence solvatochromic effects depend on the chemical structure and arrangement of the substituents. We investigated the solvatochromism of compounds **4**, **5**, **7**–**9**, and **11** in various solvents including chloroform and ethanol. The absorption maxima and emission maxima in nonpolar, aprotic polar, and protic polar solvents are listed in Table 3. The absorption maximum wavelengths of all compounds did not change significantly, but the emission maximum wavelengths of these compounds were bathochromically shifted as the polarity of the solvent increased. As a consequence, their Stokes shifts increased in polar solvents. The fluorescence intensity of pyridine compounds **4**, **7**–**9**, and **11** were stronger than that of the 2-pyridone compound **5** in all solvents (Table 2). The Φ values of **4**, **7**, and **8** in nonpolar and aprotic polar solvents were higher than those in a protic solvent (ethanol). On the other hand, dimorpholinopyridine compound **9** exhibited strong fluorescence in chloroform and DMSO. 4-Diethylamino morpholinopyridine compound **11** exhibited intense fluorescence in all solvents, indicating that it is possible to develop an efficient emissive fluorophore in solution based on 2-substituted pyridines.

*4.4 Computational analysis of the spectroscopic properties: A drastic difference in emission intensity between **4** and **5***

Regarding the absorption spectra, Table 4 lists the computed first intense λ_{max} values of all compounds. Among the tested XC functionals, the best agreement between the experimental and computed λ_{max} values were obtained using B3LYP. The computed maxima exhibited red

318 shifting in order of CAM-B3LYP < M06-2X < M06 < B3LYP < PBEPBE. The long-range
319 corrected functional CAM-B3LYP severely overestimated the vertical transition energies,
320 whereas PBEPBE underestimated the energies used to predict the λ_{max}. The inclusion of
321 solvent effects via the PCM resulted in a red shift in the B3LYP-maxima from 16 nm (**9**) to 41
322 nm (**5**) in chloroform. The B3LYP λ_{max} dependency on the two basis set (6-31+(d,p),
323 6-311++G(d,p)) is limited to a variation of 2 nm for all the compounds, as shown in Table 5.
324 Both **4** and **5** undergo considerable intramolecular electron transfer from the dialkylaminoaryl
325 moiety to methylthioaryl moiety upon S_0->S_1 excitation, as shown in Fig. 2. The two molecules,
326 however, have contrasting molecular structures derived from the steric hindrance around the
327 central single bond. For example, **4** retains a nearly flat structure, whereas **5** has a considerable
328 twist around the bond owing to the repulsion between the methylthio group and the counterpart
329 aryl group, as shown in Fig. 3.
330
331 For the fluorescence spectra, Table 6 shows the computed first intense emission maxima for all
332 compounds. The 6-31+G(d,p) basis set was uniformly employed considering the minor basis
333 set dependency mentioned above. The prediction trend is similar to that observed for
334 absorption, and λ_{max} shifted bathochromically in order of CAM-B3LYP < M06-2X < M06 <
335 B3LYP < PBEPBE. The best agreement exists between B3LYP (overestimation) and PBEPBE
336 (underestimation), excluding **4** and **5**, whose maxima were consistently predicted at shorter
337 wavelength using all XC functionals.
338
339 Notably, **4** and **5** exhibited contrasting emission intensities in solution despite only differing in
340 the modification at the nitrogen atom of the pyridine ring. We attempted to elucidate the
341 mechanism by locating the S_1-minima and the S_0/S_1 crossing seam along with the relaxation
342 pathways. The non-radiative decay channels occur along the seam of the S_0/S_1 conical

intersections (CIs), which are represented by its minimum energy points (MECIs). The S_0/S_1-MECI geometries of **4** and **5** optimized at the CASSCF(8,7)/def2-SV(P) level of theory, are shown in Fig. 4.

Our calculations clearly show the drastic differences in the energy gap between the S_1-FC and the S_0/S_1-MECI for the two molecules with severely distorted pyridine rings, as shown in Fig. 5. Compound **4** has a large gap, which is sufficient to separate the two states and prohibit the interconversion between S_1-FC and the S_0/S_1-MECI states, resulting in **4** being highly emissive. Conversely, **5** has a small gap, which allows the two states to be mutually accessible, and the S_1 excited molecule can radiationlessly return to the ground state via the S_0/S_1-MECI. The S_0 energy is not exactly identical to the S_1 energy because the optimized MECI geometry was obtained at the CASSCF(8,7)/def2-SV(P) level of theory (not B3LYP/def-TZVP).

In the solid state, the fluorescence intensity of **4** became weak, whereas that of **5** was enhanced in comparison with that in ethanol. This indicates that the intermolecular stacking interactions dominate the emission intensities of the two molecules. That is, **4**, which has a planar structure, can stack in the solid state, which activates non-radiative energy dissipation pathways, whereas the emission enhancement of **5**, which has a twisted structure, is caused by the inaccessibility of the S_0/S_1-MECI state owing to intermolecular steric hindrance. This is consistent with the observation of the emission enhancement of **9**, which has two bulky moieties, compared to the emissions of **4** and **5**.

5. Conclusion

To elucidate the influence of the keto–enol tautomerism of 2-pyridone rings on the fluorescence intensity, we synthesized two 2-pyridone tautomeric analogs, methoxypyridine

compound **4** and *N*-methylpyridone compound **5**, and demonstrated that compound **4** (enol form) shows strong fluorescence both in nonpolar and polar solvents, whereas **5** shows quite weak fluorescence. The computational analysis successfully explained the drastic difference in the fluorescence intensities between the two molecules in solution, which arises because of the energy gap between the S_1-FC and the S_0/S_1-MECI states of the two molecules. That is, **4** has a gap that is sufficiently large to separate the two states and prohibit their interconversion, thus maintaining **4** in a highly emissive state. On the other hand, **5** has a small gap that allows the two states to transition between each other, and the molecule returns to the ground state via the S_0/S_1-MECI radiationlessly. On the basis of these results, novel 2-substituted pyridine compounds **7**–**9** and **11** were synthesized from dialkylaminoacetophenones with cyanoketen *S*,*S*-acetals, and their fluorescence properties in solution and the solid state were evaluated. The substituents including phenylsulfonyl, morpholino, and 4-diethylamino groups greatly affected the fluorescence intensity in solution and the solid state. 2-Methoxypyridine compound **7** and 2-morpholinopyridine compound **8** exhibited solid-state fluorescence and a high fluorescence quantum yield in solution. Although its solution fluorescence was decreased, dimorpholinopyridine compound **9** exhibited strong fluorescence ($\Phi = 0.39$) in the solid state. In addition, a 4-diethylamino morpholinopyridine compound having 4-diethylamino group (**11**) exhibited intense fluorescence in all solvents because aggregation was prevented. These findings may be useful for the development of fluorophores exhibiting strong fluorescence in solution and the solid state.

Acknowledgments

This work was partly supported by a research grant from The Mazda Foundation.

References

[1] Chen X, Wang F, Hyun JY, Wei T, Qiang J, Ren X, Shin I, Yoon J. Recent progress in the development of fluorescent, luminescent and colorimetric probes for detection of reactive oxygen and nitrogen species. Chem Soc Rev 2016;45(10):2976–3016.

[2] Specht EA, Braselmann E, Palmer AE. A Critical and Comparative Review of Fluorescent Tools for Live-Cell Imaging. Annu Rev Physiol 2017;79:93–117.

[3] Basabe-Desmonts L, Reinhoudt DN, Crego-Calama M. Design of fluorescent materials for chemical sensing. Chem Soc Rev 2007;36(6):993–1017.

[4] Shcherbakova DM, Baloban M, Emelyanov AV, Brenowitz M, Guo P, Verkhusha VV. Bright monomeric near-infrared fluorescent proteins as tags and biosensors for multiscale imaging. Nat Commun 2016;7:12405.

[5] Zhao P, Xu Q, Tao J, Jin Z, Pan Y, Yu C, Yu Z. Near infrared quantum dots in biomedical applications: current status and future perspective. Wiley Interdiscip Rev Nanomed Nanobiotechnol 2018;10(3):e1483.

[6] Wang X, Liu L, Zhu S, Li L. Fluorescent platforms based on organic molecules for chemical and biological detection. Phys. Status Solidi RRL 2018: 1800521.

[7] He L, Lin W, Xu Q, Ren M, Wei H, Wang JY. A simple and effective "capping" approach to readily tune the fluorescence of near-infrared cyanines. Chem Sci 2015;6(8):4530–36.

[8] Sueki S, Takei R, Zaitsu Y, Abe J, Fukuda A, Seto K, Furukawa Y, Shimizu I. Synthesis of 1,4-dihydropyridines and their fluorescence properties. Eur J Org Chem 2014;2014(24):5281–301.

[9] Duan L, Qiao J, Sun Y, Qiu Y. Strategies to design bipolar small molecules for OLEDs: donor-acceptor structure and non-donor-acceptor structure. Adv Mater 2011;23(9):1137–44.

[10] Terai T, Nagano T. Small-molecule fluorophores and fluorescent probes for bioimaging. Pflugers Arch 2013;465(3):347–59.

[11] Zhu H, Fan J, Du J, Peng X. Fluorescent probes for sensing and imaging within

specific cellular organelles. Acc Chem Res 2016;49:2115–26.

[12] Li Q, Mitscher LA, Shen LL. The 2-pyridone antibacterial agents: bacterial topoisomerase inhibitors. Med Res Rev 2000;20(4):231–93.

[13] Li LN, Wang L, Cheng YN, Cao ZQ, Zhang XK, Guo XL. Discovery and characterization of 4-hydroxy-2-pyridone derivative sambutoxin as a potent and promising anticancer drug candidate: Activity and molecular mechanism. Mol Pharm 2018;15(11):4898–911.

[14] Jia H, Song Y, Yu J, Zhan P, Rai D, Liang X, Ma C, Liu X. Design, synthesis and primary biological evaluation of the novel 2-pyridone derivatives as potent non-nucleoside HBV inhibitors. Eur J Med Chem 2017;136:144–53.

[15] Isaka M, Tanticharoen M, Kongsaeree P, Thebtaranonth Y. Structures of cordypyridones A-D, antimalarial N-hydroxy- and N-methoxy-2-pyridones from the insect pathogenic fungus Cordyceps nipponica. J Org Chem 2001;66: 4803–8.

[16] Ershov OV, Fedoseev SV, Ievlev MYu, Belikov MYu. 2-Pyridone-based fluorophores: Synthesis and fluorescent properties of pyrrolo[3,4-c]pyridine derivatives. Dyes and Pigments 2016; 134, 459–64.

[17] Sellstedt M, Nyberg A, Rosenbaum E, Engström P, Wickström M, Gullbo J, Bergström S, Johansson L. B.-Å, Almqvist F. Synthesis and characterization of a multi ring-fused 2-pyridone-based fluorescent scaffold. Eur J Org Chem 2010;2010(32):6171–8.

[18] Hagimori M, Uto T, Mizuyama N, Temma T, Yamaguchi Y, Tominaga Y, Saji H. Fluorescence ON/OFF switching Zn^{2+} sensor based on pyridine–pyridone scaffold. Sens Act B Chem 2013;181:823–8.

[19] Shigemitsu Y, Hagimori M, Mizuyama N, Wang BC, Tominaga Y. Theoretical interpretations of electronic and fluorescence spectra of new 2(1H)-pyridone derivatives in solution and solid state. Dyes and Pigments 2013;99(3): 940–9.

[20] Hagimori M, Shigemitsu Y, Murakami R, Yokota K, Nishimura Y, Mizuyama N,

Wang BC, Tai CK, Wang SL, Shih TL, Wu KD, Huang ZS, Tseng SC, Lu JW, Wei HH, Nagaoka J, Mukai T, Kawashima S, Kawashima K, Tominaga Y. 2-Pyridone-based fluorophores containing 4-dialkylamino-phenyl group: Synthesis and fluorescence properties in solutions and in solid state. Dyes Pigm 2016;124:196–202.

[21] Wong MW, Wiberg KB, Frisch MJ. Solvent effects. 3. Tautomeric equilibria of formamide and 2-pyridone in the gas phase and solution: an ab initio SCRF study. J Am Chem Soc 1992;114:1645–52.

[22] Forlani L, Cristoni G, Boga C, Todesco PE, Del Vecchio E, Selva S, Monari M. Reinvestigation of tautomerism of some substituted 2-hydroxypyridines. Arkivoc 2002;XI:198–215.

[23] Hejazi SA, Osman OI, Alyoubi AO, Aziz SG, Hilal RH. The Thermodynamic and Kinetic Properties of 2-Hydroxypyridine/2-Pyridone Tautomerization: A Theoretical and Computational Revisit. Int J Mol Sci 2016;17(11): E1893.

[24] Frank J, Katritzky AR. Tautomeric pyridines. Part XV. Pyridone–hydroxypyridine equilibria in solvents of differing polarity. J Chem Soc Perkin Trans 2 1976:1428–31.

[25] El-Kemary M, Rettig W. Multiple Emission in Coumarins with Heterocyclic Substituents. Phys Chem Chem Phys 2003;5:5221–8.

[26] Yamaguchi E, Wang C, Fukazawa A, Taki M, Sato Y, Sasaki T, Ueda M, Sasaki N, Higashiyama T, Yamaguchi S. Environment-sensitive fluorescent probe: a benzophosphole oxide with an electron-donating substituent. Angew Chem Int Ed Engl 2015;54(15):4539–43.

[27] Hagimori M, Mizuyama N, Shigemitsu Y, Wang BC, Tominaga Y. Development of Fluorescent 2-Pyrone Derivatives Using Ketene Dithioacetals for Organic EL Devices. Heterocycles 2009;78(3):555–70.

[28] Sun Y, Sun Y, Zhao S, Cao D, Guan R, Liu Z, Yu X, Zhao X. Efficient solution- and solid-state fluorescence for a series of 7-diethylaminocoumarin amide compounds.

Asian J Org Chem 2018;7:197–202.

[29] Gaussian 09, Rev. A.2. Frisch MJ, Trucks GW, Schlegel HB, Scuseria GE, Robb MA, Cheeseman JR, et al: Gaussian, Inc. Pittsburgh PA.

[30] Becke, A.D. Becke's three parameter hybrid method using the LYP correlation functional. J. Chem. Phys. 1993;98: 5648-52.

[31] Yanai, T., Tew, D. P., & Handy, N. C. A new hybrid exchange–correlation functional using the Coulomb-attenuating method (CAM-B3LYP). Chemical Physics Letters 2004;393 (1-3), 51-7.

[32] Adamo, C., Barone, V. Toward reliable density functional methods without adjustable parameters: The PBE0 model. J. Chem. Phys. 1999; 110: 6158-69

[33] Zhao,Y. and Truhlar, D.G. The M06 suite of density functionals for main group thermochemistry, thermochemical kinetics, noncovalent interactions, excited states, and transition elements: two new functionals and systematic testing of four M06-class functionals and 12 other functionals. Theor. Chem. Acc. 2008; 120 :215-41.

[34] Yarkony, D. R. Conical intersections: Diabolical and often misunderstood. Accounts of chemical research, 1998;31(8): 511-8.

[35] MOLPRO, version 2015.1, a package of ab initio programs, H.-J. Werner, P. J. Knowles, G. Knizia, F. R. Manby, M. Schütz, and others , see http://www.molpro.net.

[36] TURBOMOLE V7.1 2017, a development of University of Karlsruhe and Forschungszentrum Karlsruhe GmbH, 1989-2007,TURBOMOLE GmbH, since 2007; available fromhttp://www.turbomole.com.

[37] Hagimori M, Matsui S, Mizuyama N, Yokota K, Nagaoka J, Tominaga Y. Novel synthesis of 4H-quinolizine derivatives using sulfonyl ketene dithioacetals. Eur J Org Chem 2009;2009(33):5847–53.

[38] Hagimori M, Mizuyama N, Yokota K, Nishimura Y, Suzuta M, Tai CK, Wang BC, Wang SL, Shih TL, Wu KD, Huang ZS, Tseng SC, Chen CY, Lu JW, Wei HH, Kawashima K, Kawashima S, Tominaga Y. Synthesis of

6-(4-diethylamino)phenyl-2-oxo-2H-pyran-3-carbonitorile derivatives and their fluorescence in solid state and in solutions. Dyes Pigm 2012;92(3):1069–74.

528

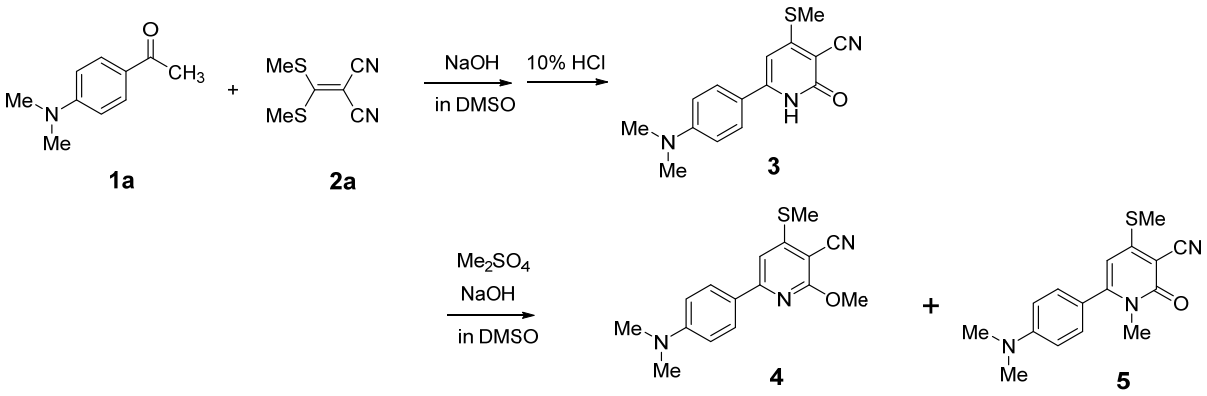

Scheme 1. Synthesis of methoxypyridine **4** and *N*-methylpyridone **5**.

529

530

531

532

Table 1. UV and fluorescence data for **3–5** in solution ($CHCl_3$ and ethanol) and the solid state.

Compounds	Dissolved in $CHCl_3$			Dissolved in ethanol			Solid	
	λ_{max} (:nm)[a]	Em_{max} (nm)[b]	Φ[c]	λ_{max} (nm)[a]	Em_{max} (nm)[b]	Φ[c]	Em_{max} (nm)[b]	Φ[c]
3[d]	410	487	0.90	408	511	0.11	589	0.17
4	386	461	>0.99	384	491	0.61	524	0.03
5	384	461	0.12	384	491	0.05	533	0.18

[a]Concentration: 10^{-5} M. [b]Each emission was measured using excitation wavelengths. [c]Quantum yields were determined using an Absolute PL Quantum Yield Measurement System (C9920-01) from Hamamastu Photonics. [d]The UV and fluorescence data are listed in Ref. [20].

533

534

535

536

537

538

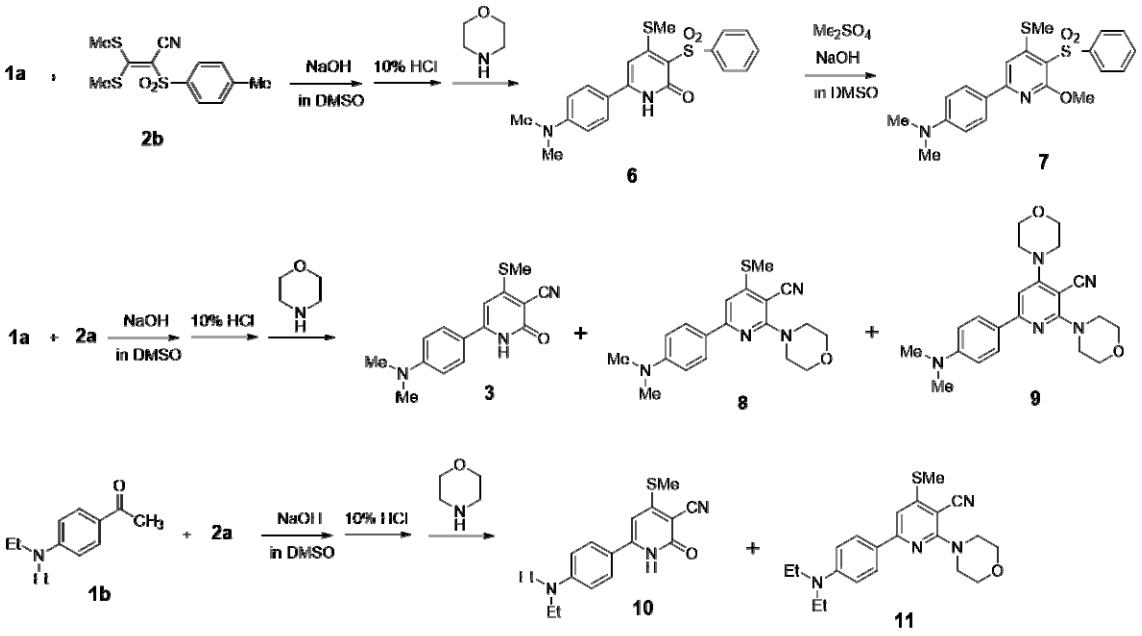

Scheme 2. Synthesis of 2-substituted pyridine compounds **7–9** and **11**.

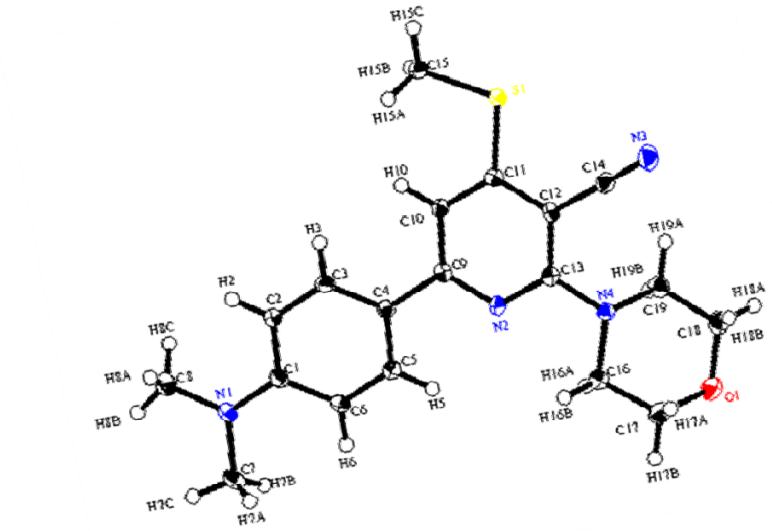

Fig. 1. ORTEP drawing of **8**.

546

Table 2. UV and fluorescence data for 2-substituted pyridine compounds **7–9** and **11** in solution ($CHCl_3$ and ethanol) and in the solid state.

Compounds	Dissolved in $CHCl_3$			Dissolved in ethanol			Solid	
	λ_{max} (nm)[a]	EM_{max} (nm)[b]	Φ[c]	λ_{max} (nm)[a]	EM_{max} (nm)[b]	Φ[c]	EM_{max} (nm)[b]	Φ[c]
7	386	455	0.95	386	487	0.62	475	0.15
8	388	459	0.83	386	491	0.59	436	0.12
9	348	410	0.64	346	426	0.23	441	0.39
11	386	435	0.87	382	465	0.88	491	0.19

[a]Concentration: 10^{-5}M. [b]Each emission was measured using excitation wavelengths. [c]This quantum yields were determined by using Absolute PL Quantum Yield Measurement System (C9920-01) of Hamamastu Photonics..

547

548

Table 3. UV-absorption and fluorescence properties of **4, 5, 7–9** and **11** in various solvents.

	λ_{max} (nm) (log e)					
Solvent	**4**	**5**	**7**	**8**	**9**	**11**
benzene	384 (4.68)	384 (4.64)	384 (4.46)	386 (4.68)	350 (4.52)	384 (4.59)
chloroform	386 (4.69)	386 (4.64)	386 (4.48)	388 (4.69)	348 (4.60)	386 (4.59)
acetone	380 (4.71)	384 (4.66)	382 (4.50)	386 (4.71)	346 (4.57)	380 (4.62)
ethanol	384 (4.67)	384 (4.66)	386(4.47)	386 (4.75)	346 (4.52)	382 (4.58)
acetonitrile	382 (4.68)	384 (4.65)	384 (4.48)	382 (4.69)	348 (4.54)	382 (4.59)
DMSO	392 (4.68)	392 (4.66)	392 (4.51)	392 (4.70)	352 (4.52)	388 (4.62)

	EM_{max} (nm) (Φ)					
Solvent	**4**	**5**	**7**	**8**	**9**	**11**
benzene	453 (0.92)	453 (0.07)	445 (0.87)	449 (0.78)	400 (0.28)	425 (>0.99)
chloroform	461 (>0.99)	461 (0.12)	455 (0.95)	459 (0.83)	410 (0.64)	435 (0.87)
acetone	489 (0.80)	489 (0.06)	485 (0.92)	485 (0.74)	410 (0.26)	447 (>0.99)
ethanol	491 (0.61)	491 (0.05)	487 (0.62)	491 (0.59)	426 (0.23)	465 (0.88)
acetonitrile	495 (0.71)	495 (0.06)	491 (0.84)	489 (0.69)	410 (0.33)	459 (>0.99)
DMSO	501 (0.64)	503 (0.05)	497 (0.72)	497 (0.63)	416 (0.76	465 (0.94)

549

550

Table 4 Computed absoption λ_{max} (nm) and Oschillator strength f using several XC-functionals

Compounds	B3LYP		B3LYP in $CHCl_3$		CAM-B3LYP		PBEPBE		M06		M06-2X	
	λ_{max}	f	λ_{max}	f	λ_{max}	f	λ_{max}	f	λ_{max}	f	λ_{max}	f
4	377	0.77	409	0.93	330	0.97	440	0.55	366	0.82	331	0.98
5	374	0.54	415	0.57	331	0.65	447	0.32	362	0.59	331	0.67
7	370	0.73	396	0.87	323	0.97	444	0.40	360	0.78	325	0.97
8	380	0.57	403	0.85	335	0.67	437	0.43	370	0.62	337	0.69
9	363	0.44	379	0.81	319	0.65	414	0.34	352	0.56	320	0.67
11	382	0.63	404	0.88	336	0.71	441	0.39	371	0.66	337	0.73

Table 5 Computed absoption λ_{max} (nm) and Oschillator strength f using the two basis sets

Compounds	6-31+G**		6-311++G**	
	λ_{max}	f	λ_{max}	f
4	377	0.77	378	0.77
5	374	0.54	375	0.54
7	370	0.73	372	0.73
8	380	0.57	381	0.56
9	363	0.44	364	0.44
11	382	0.63	383	0.62

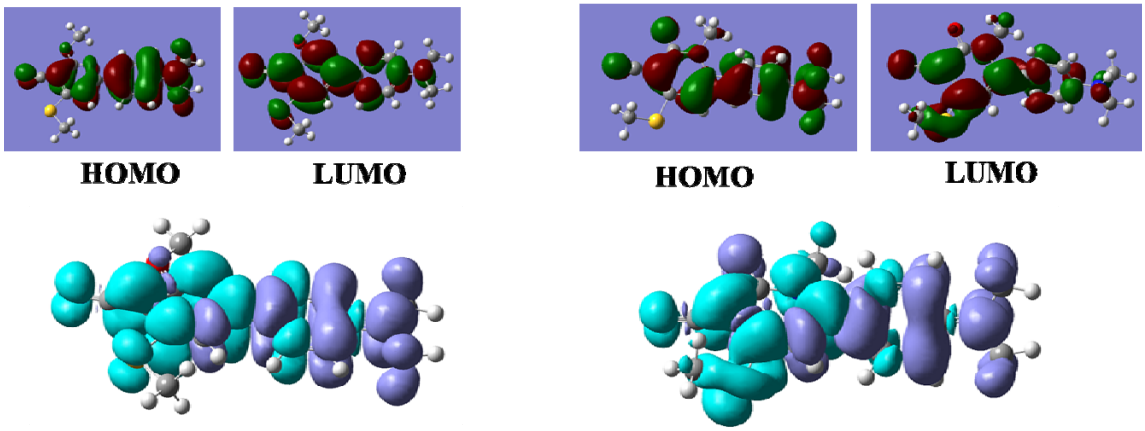

Fig. 2 HOMO, LUMO and S_0/S_1-electron density difference of **4** (left) and **5** (right)

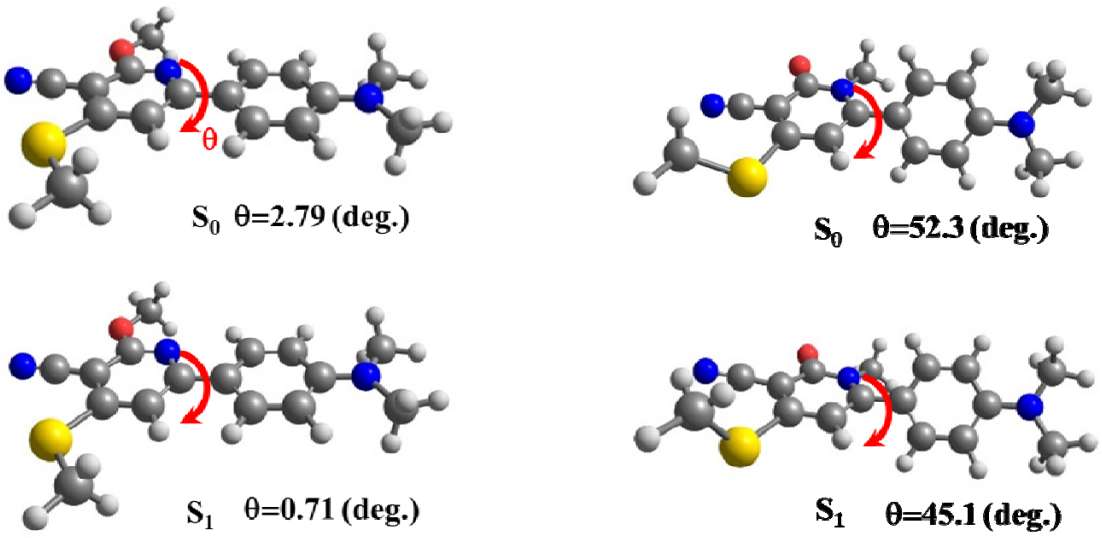

Fig. 3 The S_0, S_1 optimized geometry of **4** (left) and **5** (right)

Table 6 Computed fluorescence λ_{max} (nm) and Oschillator strength f using several XC-functionals

Compounds	B3LYP		CAM-B3LYP		PBEPBE		M06		M06-2X	
	λ_{max}	f	λ_{max}	f	λ_{max}	f	λ_{max}	f	λ_{max}	f
4	351	0.03	337	0.00	415	0.02	349	0.03	312	0.03
5	363	0.24	349	0.26	460	0.02	435	0.02	352	0.18
7	386	0.95	344	1.11	446	0.69	377	0.98	345	1.12
8	392	0.82	347	1.00	457	0.47	383	0.86	348	1.01
9	372	0.79	334	1.03	421	0.57	365	0.9	335	1.03
11	402	0.77	347	1.00	482	0.51	388	0.83	348	0.99

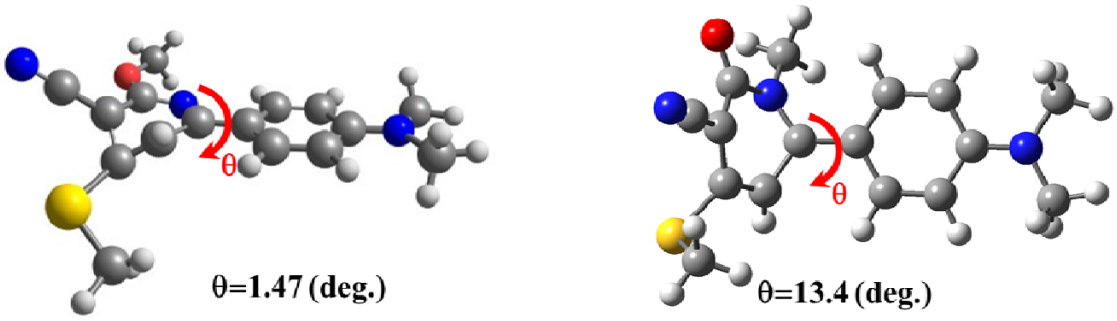

589 **Fig. 4** MECI geometries of **4** (left) and **5** (right)

590

591

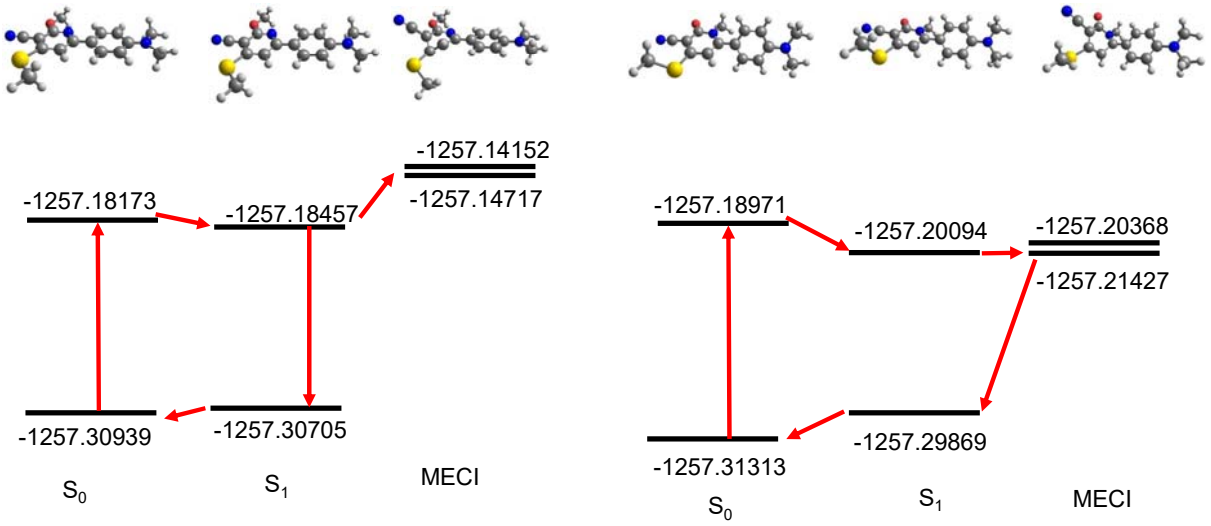

592 **Fig. 5** The energy diagram of **4** (left) and **5** (right) (The energies in atomic unit.)

593

594

595